고해상도 Sentinel-2 위성 자료와 지형효과를 고려한 식생지수 기반의 산림 식생 생장패턴 비교

유승헌[1], 정성찬[2*]

[1]서울대학교 농업생명과학대학 조경.지역시스템공학부 조경학전공
[2]서울대학교 환경대학원 협동과정 조경학

(2024년 01월 29일 접수; 2024년 03월 17일 수정; 2024년 05월 07일 수락)

A Comparative Study of Vegetation Phenology Using High-resolution Sentinel-2 Imagery and Topographically Corrected Vegetation Index

Seungheon Yoo[1], Sungchan Jeong[2*]

[1]*Department of Landscape Architecture and Rural Systems Engineering, Seoul National University*
[2]*Interdisciplinary Program in Landscape Architecture, Seoul National University*

(Received January 29, 2024; Revised March 17, 2024; Accepted May 07, 2024)

ABSTRACT

Land Surface Phenology (LSP) plays a crucial role in understanding vegetation dynamics. The near-infrared reflectance of vegetation (NIRv) has been increasingly adopted in LSP studies, being recognized as a robust proxy for gross primary production (GPP). However, NIRv is sensitive to the terrain effects in mountainous areas due to artifacts in NIR reflectance cannot be canceled out. Because of this, estimating phenological metrics in mountainous regions have a substantial uncertainty, especially in the end of season (EOS). The topographically corrected NIRv (TCNIRv) employs the path length correction (PLC) method, which was deduced from the simplification of the radiative transfer equation, to alleviate limitations related to the terrain effects. TCNIRv has been demonstrated to estimate phenology metrics more accurately than NIRv, especially exhibiting improved estimation of EOS. As the topographic effect is significantly influenced by terrain properties such as slope and aspect, our study compared phenology metrics estimations between south-facing slopes (SFS) and north-facing slopes (NFS) using NIRv and TCNIRv in two distinct mountainous regions: Gwangneung Forest (GF) and Odaesan National Park (ONP), representing relatively flat and rugged areas, respectively. The results indicated that TCNIRv-derived EOS at NFS occurred later than that at SFS for both study sites (GF : DOY 266.8/268.3 at SFS/NFS; ONP : DOY 262.0/264.8 at SFS/NFS), in contrast to the results obtained with NIRv (GF : DOY 270.3/265.5 at SFS/NFS; ONP : DOY 265.0/261.8 at SFS/NFS). Additionally, the gap between SFS and NFS diminished after topographic correction (GF : DOY 270.3/265.5 at SFS/NFS; ONP : DOY 265.0/261.8 at SFS/NFS). We conclude that TCNIRv exhibits discrepancy with NIRv in EOS detection considering slope orientation. Our findings underscore the necessity of topographic correction in estimating photosynthetic phenology, considering slope orientation, especially in diverse terrain conditions.

Key words: Phenology, Topographic correction, Vegetation index, TCNIRv

---

* Corresponding Author : Sungchan Jeong
(sungchanm@snu.ac.kr)

I. Introduction

Land Surface Phenology (LSP) is a field of study that focuses on the plant growth stages in vegetated land surfaces using remote sensing technologies (de Beurs & Henebry, 2004; Yang & Fan, 2023; Zeng et al., 2020). These phenological metrics encompass the start of the growing season (SOS) and the end of the growing season (EOS). These serve as proxies for the spring and autumn phenophases, facilitating the vegetation phenological dynamics monitoring at the landscape level (Karami et al., 2018; Rodriguez-Galiano et al., 2015). Satellite-based LSP plays a pivotal role in monitoring plant phenology due to the advantage of expansive coverage compared to in situ measurements taken with radiometric instruments, flux tower, and airborne observations (Dash & Ogutu, 2016; Wang et al., 2017).

The analysis of LSP primarily relies on vegetation indices (VIs) and other biophysical variables derived from optical remote sensing datasets (Caparros-Santiago et al., 2021). Recent studies have established that near-infrared reflectance of vegetation (NIRv) represents a more suitable option for extracting phenology metrics compared to other VIs such as the normalized difference vegetation index (NDVI) (Badgley et al., 2017; Yin et al., 2020a). While NDVI is widely employed for LSP studies (Caparros-Santiago et al., 2021), it has following limitations: NDVI is sensitive to variations in soil background and understories, resulting in the insensitivity to gross primary production (GPP), particularly in areas with high biomass due to saturation effects (Huete et al., 2002). The near-infrared reflectance (NIR) was known to be a more robust proxy of GPP than NDVI, if the vegetated signal is separated from non-vegetated reflectance (Badgley et al., 2017). NIRv is the production of NDVI and NIR, and it is known that NIRv specifically captures NIR from vegetation and minimizes the influence of background soil, thereby addressing saturation problems in dense vegetation (Badgley et al., 2017; Baldocchi et al., 2020). SOS

estimated from NIRv shows good consistency with GPP-derived estimates but EOS estimated from NIRv lags significantly behind GPP-derived EOS (Yang et al., 2022). It is grounded in the primary factors that constrain photosynthesis, exhibiting variations across distinct growth stages. During spring, the chlorophyll content predominantly influences the rate of carbon sequestration, making NIRv sensitive to chlorophyll content (Raddi et al., 2022) and enabling a reliable estimation of the SOS. In autumn, plant photosynthesis encounters limitations due to the diminishing availability of illumination conditions caused by the rapid decline in solar radiation (Zhang et al., 2020). Consequently, even though chlorophyll is still present, plants are unable to harness sufficient light for photosynthesis. This delay results in a tardy estimation of the EOS through NIRv extraction.

In mountainous areas, topography significantly affects illumination conditions at sloped surfaces (Wen et al., 2009) and makes phenology monitoring difficult. The band ratio-based VIs (e.g., NDVI) can partially alleviate such distortion due to the similar topographic influences in relative terms on the red and near infrared (NIR) spectral band reflectances. However, VIs without a band ratio format such as NIRv, prove to be more sensitive to topographic effects (Chen et al., 2020). The path length correction (PLC) is one of the topographic correction methods based on the classic radiative transfer equation (Yin et al., 2018). The PLC method aims to convert the reflectance from an inclined surface to its equivalent over a horizontal surface (Yin et al., 2018). The PLC method has a solid physical foundation as it relies on physics-based parameters rather than empirical parameters. Additionally, it demonstrates high topographic correction performance through simple mathematic calculation (Chen et al., 2023a; Yin et al., 2020b).

The topographically corrected NIRv (TCNIRv) is suggested as one of the solutions for topographic effects using PLC methods (Chen et al., 2023b). The recent studies suggested that TCNIRv shows high co-relationship with GPP (Chen et al., 2022) and

makes good estimation of phenological metrics, especially improving EOS estimation performance (Chen *et al*., 2023b).

But to the best of our knowledge, there are only few LSP studies using TCNIRv and the photosynthetic phenology with respect to slope orientation derived from TCNIRv is still not clear even though TCNIRv calculation is based on such topographic properties. We propose the need to separate the results by slope orientation to precisely observe the impact of topographic correction on phenology metrics extraction. For this study, we pursued two objectives : (1) clarify the difference between phenology metrics derived from NIRv and TCNIRv and (2) whether the phenology metrics at south-facing-slope (SFS) statistically differs from that at north-facing-slope (NFS).

II. Materials and Methods

2.1. Study area

We conducted the research in South Korea, which is located in the Northeast Asia. We selected two study areas as mountainous areas with different topography aligned on similar latitude (Fig. 1) to compare the effect of topographic correction depending on the topography features (i.e., slope and aspect). Gwangneung Forest (GF), relatively flat and simple terrain with elevation ranging from 90 to 428 m (Fig. 1(a)). The average elevation at GF is about 184.2m and mean slope is about 13.9°. Odaesan National Park (ONP) has dynamic elevation level ranging from 234 to 1561m (Fig. 1(b)). The average elevation at ONP is about 962.0m and mean slope is about 24.3°.
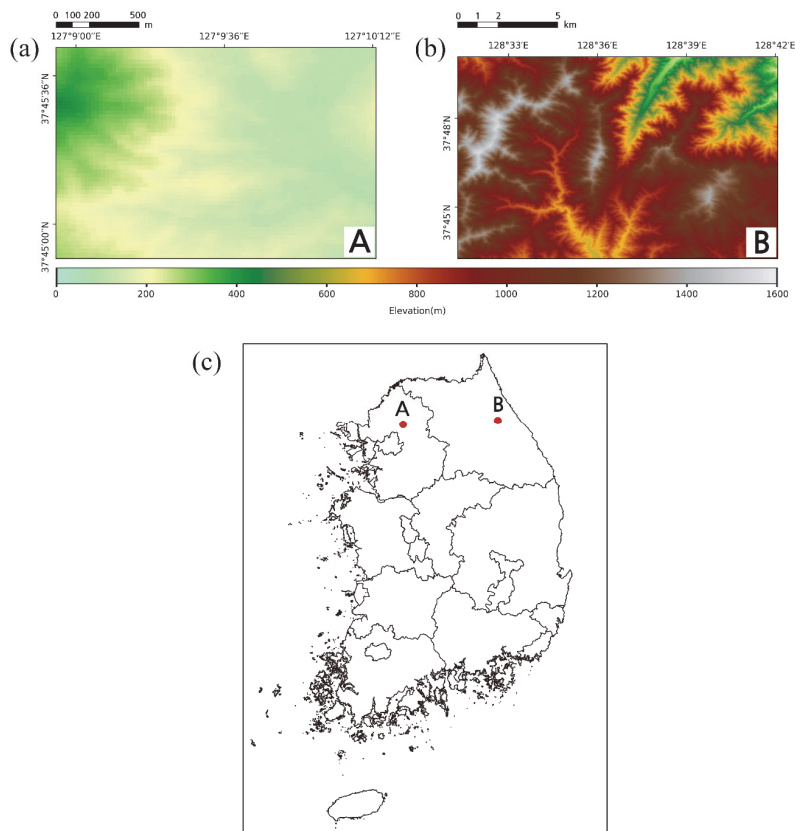

Fig. 1. Elevation map for the study areas (a) Gwangneung Forest and (b) Odaesan National Park. (c) GF and ONP are on similar latitudes, but have significant differences in topographic features.

2.2. Data Acquisition and Preparation

We selected the images with a higher spatial resolution than those typically adopted in LSP studies to observe the topographic effect on phenology estimation in detail, considering the topographic features. Sentinel-2 L2 images have 10m spatial resolution with 5-day frequency, which is atmospherically corrected with Sen2Cor algorithm. We acquired Sentinel-2 L2 images from Google Earth Engine (GEE) spanning from 2019 to 2022. We filtered out cloud contaminated pixels by GEE algorithms and only the images with at least 70% of clear pixels were retained for the research. We illustrated the day of the year (DOY) of the adopted data in Fig. 2.

We needed 10m resolution Digital Elevation Model (DEM) to overlap with Sentinel-2 L2 images. We obtained digital topographic map in shape file from National Spatial Data Infrastructure Portal and used ArcGIS 10.5 to create DEM in 10m pixel size.
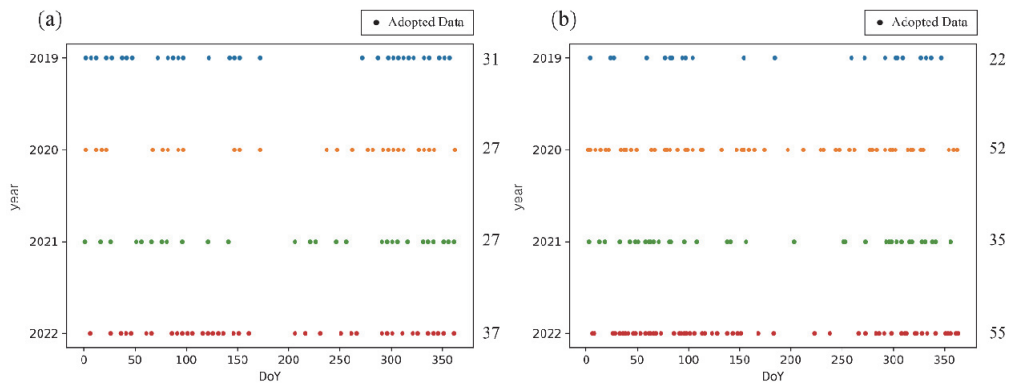

Fig. 2. The distribution of the Sentinel-2 L2 data which are adopted for the study, according to DOY. Each dot represents the DOY of the data adopted for each year. The data with more than 30% cloud pixels are excluded. (a) and (b) shows the data distribution for GF and ONP, respectively.
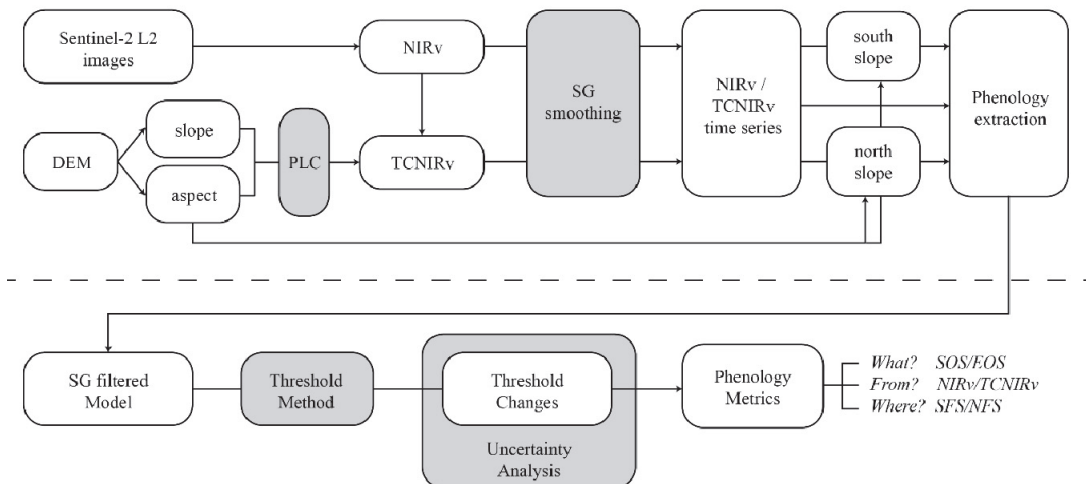

Fig. 3. Process flowchart for (1) NIRv and TCNIRv construction, (2) smoothing methods for time series, (3) division to SFS and NFS, (4) phenology extraction methods, analyzing uncertainty, and finally comparing phenology metrics focusing on three main points : SOS/EOS, NIRv/TCNIRv, SFS/NFS.

2.3. Methods

We calculated slope and aspect from DEM with Horn's algorithm (Horn, 1981) from 10m resolution DEM. These are used for calculating TCNIRv with NIRv derived from Sentinel-2 L2 images by PLC method. Then we smoothed NIRv and TCNIRv time series with Savitzky-Golay filter and applied threshold method for phenology extraction. Then we checked the uncertainties for phenology metrics by changing threshold in set range (Wang *et al.*, 2019). Finally, we calculated SOS and EOS at NFS and SFS derived from NIRv and TCNIRv for each pixel and compared the distribution of those.

2.3.1. NIRv and TCNIRv calculation

NIRv and TCNIRv is calculated with following equations :

$$NIRv = \frac{NIR - Red}{NIR + Red} \cdot NIR \qquad (1)$$

$$TCNIRv = \frac{S(\Omega_1) + S(\Omega_2)}{S_t(\Omega_1) + S_t(\Omega_2)} \cdot NIRv \qquad (2)$$

TCNIRv is calculated with PLC method, multiplying correction coefficient to NIRv. Ω_1 is the solar direction and Ω_2 is the viewing direction, including informations of zenith angle and azimuth angle. S and S_t are the path length on different topographic features, flat and sloping terrain, respectively. In Equation (2), we multiply NIRv by the ratio of the total path length over a horizontal surface to the total path length over an inclined surface under the same conditions except for the slope of the terrain. The factors in the correcting coefficient is calculated with following equations :

$$S(\theta) = 1/cos\,\theta \qquad (3)$$

$$S_t(\theta, \varphi, \alpha, \beta) = \frac{1}{cos\theta \cdot (1 - tan\alpha \cdot cos(\varphi - \beta) \cdot tan\theta)} \qquad (4)$$

θ is zenith angle and φ is azimuth angle, using these of solar angles for $S(\Omega_1)$ and $S_t(\Omega_1)$, and viewing angles for $S(\Omega_2)$ and $S_t(\Omega_2)$. α and β stand for slope and aspect angles calculated from DEM, respectively.

2.3.2. SFS and NFS

We targeted only south and north facing slopes to check the impact of the topographic correction to the phenology pattern. As we calculated aspect from DEM, we defined SFS as 90°-270°, NFS as 0°-90° and 270°-360°. Fig. 4 shows the pixels of SFS and NFS for each study site.
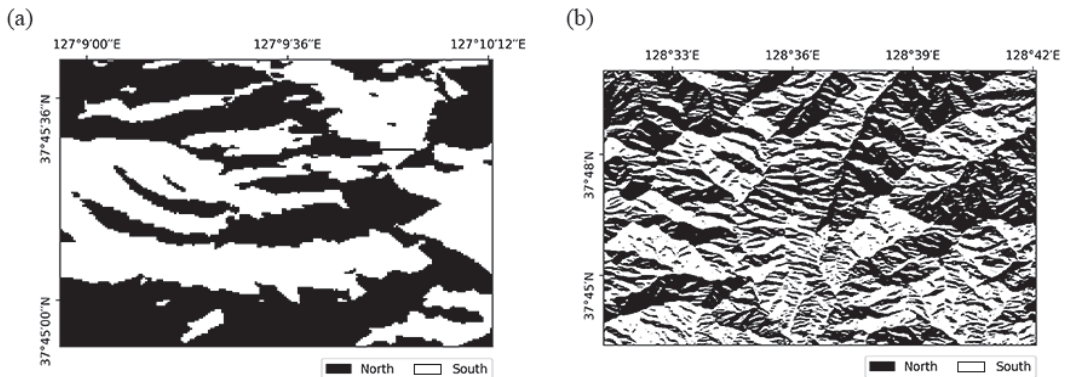

Fig. 4. Denoting the pixels of north and south slope. (a) and (b) are reclassified DEM for GF and ONP, respectively. The black pixels and white pixels are representing north side and south side of the mountain, respectively.

2.4. Land Surface Phenology Metrics Calculation

Sentinel-2 offers relatively high temporal frequencies as 5-day interval, but substantial amount of data, particularly during the summer, is discarded due to cloud contaminations (Fig. 2). To mitigate the noise impacts, we applied the Savitzky-Golay filter to smooth NIRv and TCNIRv time series. Then, we calculated SOS and EOS using a threshold expressed as a percentage, considering the minimum and maximum values of VI (White *et al*., 1997). SOS is defined as DOY on which VI reaches a specific upward threshold, while EOS is determined as the point at which the adjusted curve crosses a specific downward threshold (Caparros-Santiago *et al*., 2021).

However, the threshold method has a limitation that the threshold is arbitrary, and phenology metrics can be altered by the threshold, even using the same VI time series data (Caparros-Santiago *et al*., 2021). Focusing on the differences of phenology metrics between SFS and NFS, our primary objective was to observe the distributions of SOS and EOS derived from various thresholds. We calculated phenology metrics by adjusting thresholds from 15% to 50% with a step of 0.1% and analyzed their distributions. The lower and upper limits were set at 15% and 50%, respectively, based on the understanding that the standard deviation of estimated phenology metrics become stable for thresholds over 15% (Wang *et al*., 2019), and the 50% threshold is commonly chosen value for phenology extraction due to its reliable performance in estimating vegetation growth states (Wang *et al*., 2020). Then, we conducted t-tests for the calculated groups to ascertain whether a statistically significant difference exists. 'n.s.' indicates no significant differences between the two slopes, while '*' denotes significant differences between them (p-value < 0.05). Following the verification of statistical differences in phenology metrics between SFS and NFS, we analyzed the specific disparity between them by comparing the exact DOY calculated with a 50% threshold.

III. Result

3.1. Phenology metrics derived from NIRv and TCNIRv

We summarized the dates of SOS and EOS at GF and ONP at Table 1 and Table 2, respectively. We observed that both SOS and TCNIRv-derived EOS are relatively moved up compared to those derived from NIRv for both study areas. The EOS gap was notably different between these areas, i.e., the EOS gap at GF was -0.8 days while EOS gap at ONP was -2.5 days. This result implies that topographic effects significantly impact to EOS estimation.

3.2. Phenology metrics with respect to slope orientation

3.2.1. Phenology metrics uncertainties

Before examining the exact differences in phenology metrics between SFS and NFS, we demonstrated that there are significant differences in phenology metrics between them. We illustrated the phenology metrics calculated with NIRv/TCNIRv in GF and ONP at Fig. 6 and Fig. 7, respectively. At GF, NIRv-derived SOS exhibits no significant differences between SFS and NFS. Similarly, TCNIRv-derived SOS also shows no significant differences between SFS and NFS, or it is one day faster at SFS than NFS. We found the significant differences in estimate of EOS : NIRv-derived estimate of EOS was earlier at NFS than SFS, but TCNIRv-derived EOS was considerably delayed at NFS compared to SFS for both study sites.

3.2.2. Phenology metrics comparison

We examined the exact DOY for phenology metrics with a 50% threshold. The results for GF are presented in Table 3 and Table 4, and the results for ONP are presented in Table 5 and Table 6. Additionally, we calculated the gap between SFS and NFS by subtracting SFS metrics from NFS metrics. Both NIRv-derived and TCNIRv-derived SOS appear relatively stable compared to EOS for both areas. At
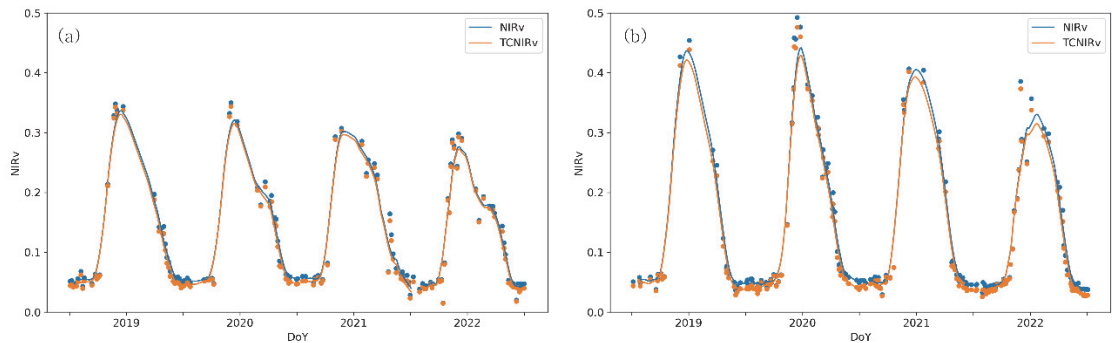
Fig. 5. (a) and (b) are NIRv and TCNIRv time series smoothed by SG filter at GF and ONP, respectively.

Table 1. Phenology metrics derived from NIRv and TCNIRv at GF. We observed that SOS and TCNIRv-derived EOS are both preceding to those derived from NIRv

GF	SOS (DOY)			EOS (DOY)		
	NIRv	TCNIRv	Gap	NIRv	TCNIRv	Gap
2019	119.0	118.0	-1.0	268.0	267.0	-1.0
2020	121.0	120.0	-1.0	274.0	272.0	-2.0
2021	106.0	106.0	0.0	267.0	268.0	+1.0
2022	115.0	115.0	0.0	271.0	270.0	-1.0
Average	115.3	114.8	-0.5	270.0	269.3	-0.8

Table 2. Phenology metrics derived from NIRv and TCNIRv at ONP. We observed that SOS and TCNIRv-derived EOS are both preceding to those derived from NIRv

ONP	SOS (DOY)			EOS (DOY)		
	NIRv	TCNIRv	Gap	NIRv	TCNIRv	Gap
2019	129.0	128.0	-1.0	270.0	266.0	-4.0
2020	141.0	140.0	-1.0	237.0	238.0	+1.0
2021	123.0	123.0	0.0	267.0	263.0	-4.0
2022	134.0	133.0	-1.0	270.0	267.0	-3.0
Average	131.8	131.0	-0.8	261.0	258.5	-2.5

GF, the average NIRv-derived EOS at SFS is DOY 270.3, and the NIRv-derived EOS at NFS is DOY 265.5, resulting in an average gap of about -4.8 days. The average TCNIRv-derived EOS at SFS is DOY 266.8, and the TCNIRv-derived EOS at NFS is DOY 268.3, resulting in an average gap of about 1.5 days. At ONP, the average NIRv-derived EOS at SFS is 265, and the NIRv-derived EOS at NFS is 261.8, resulting in an average gap of -3.3 days. The average

TCNIRv-derived EOS at SFS is DOY 262, and the TCNIRv-derived EOS at NFS is DOY 264.8, resulting in an average gap of about 2.8 days. We observed that NIRv-derived EOS is earlier at NFS than SFS, whereas TCNIRv-derived EOS is earlier at SFS than NFS. Additionally, an absolute difference between SFS and NFS is larger for NIRv-derived EOS compared to TCNIRv-derived EOS.
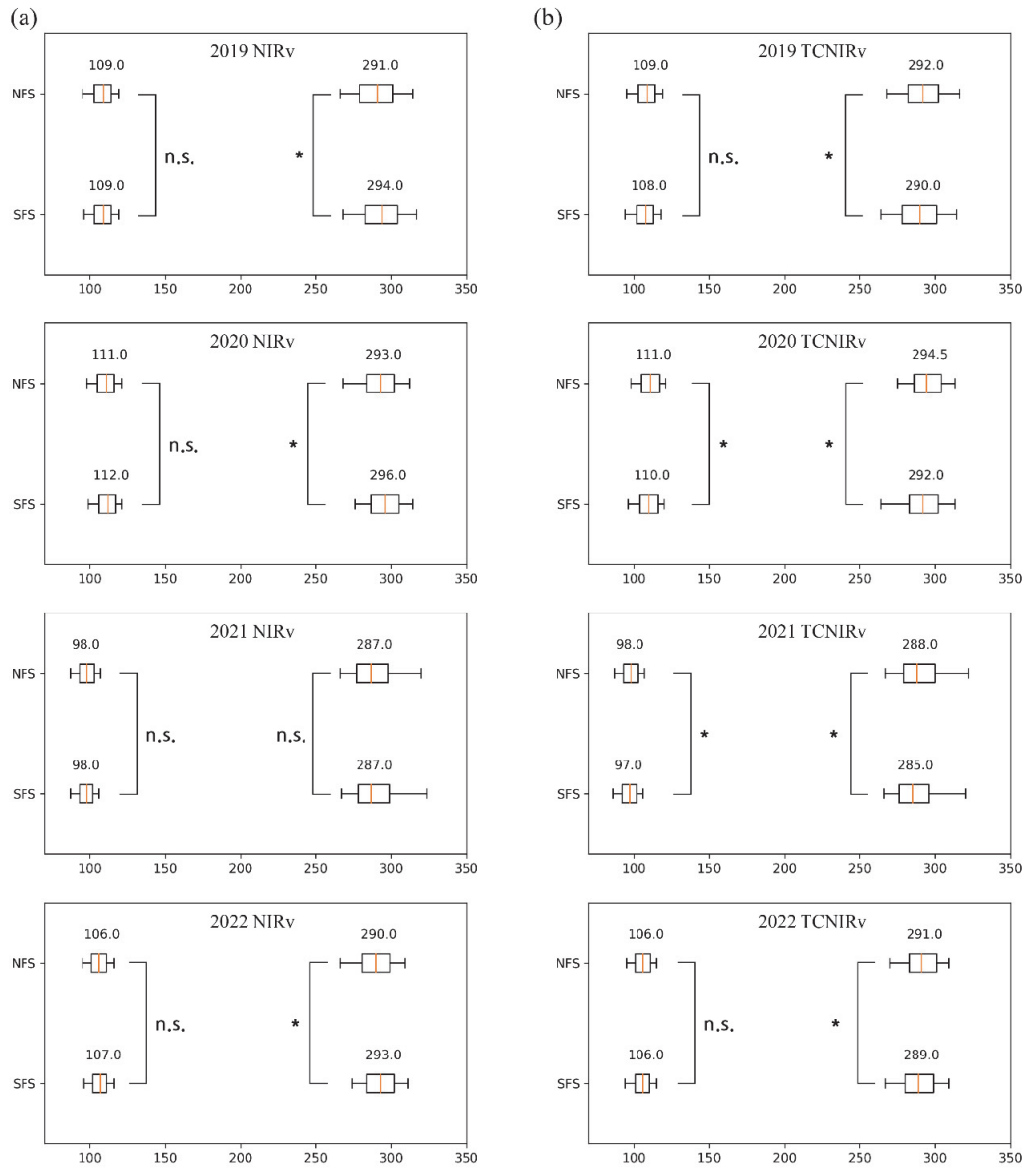
(a)

(b)

Fig. 6. Boxplots representing the distributions of SOS and EOS for GF, obtained by varying thresholds from 15% to 50% with a step of 0.1%. (a) and (b) present results derived from NIRv and TCNIRv, respectively. NIRv-derived EOS occurs earlier at NFS than SFS, but TCNIRv-derived EOS occurs later at NFS than SFS.

Fig. 7. Boxplots representing the distributions of SOS and EOS for ONP, obtained by varying thresholds from 15% to 50% with a step of 0.1%. (a) and (b) present results derived from NIRv and TCNIRv, respectively. NIRv-derived EOS occurs earlier at NFS than SFS, but TCNIRv-derived EOS occurs later at NFS than SFS.
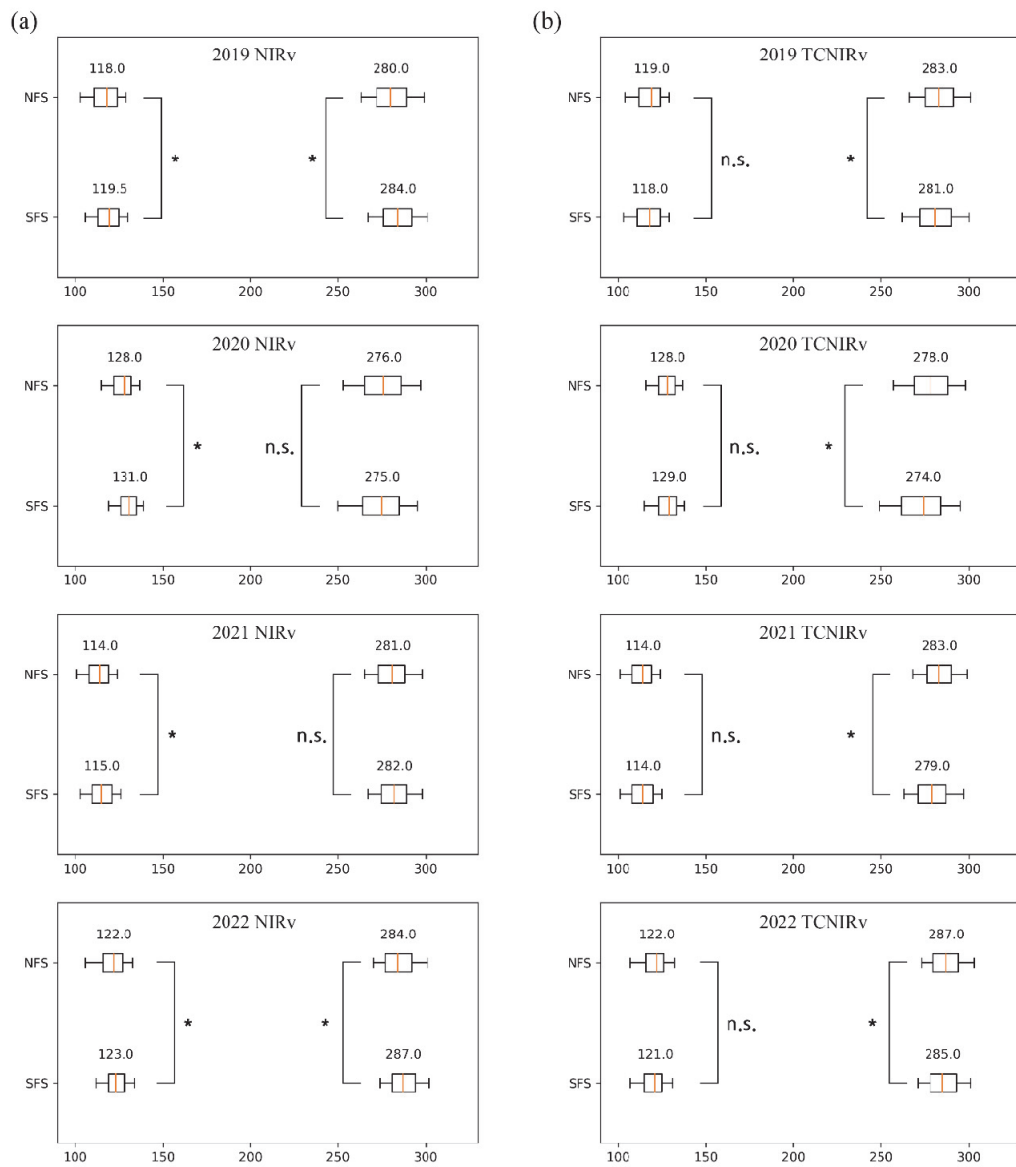
Table 3. Phenology metrics derived from NIRv for GF, 2019-2022. The gap is calculated as the metrics of NFS – SFS. Note that EOS at NFS is averagely 4.8 days earlier than that at SFS

GF (NIRv)	SOS (DOY)			EOS (DOY)		
	SFS	NFS	Gap	SFS	NFS	Gap
2019	117.0 (± 12.1)	118.0 (± 7.5)	+1.0	270.0 (± 21.8)	268.0 (± 18.3)	-2.0
2020	122.0 (± 14.3)	122.0 (± 11.5)	0.0	270.0 (± 28.6)	265.0 (± 27.1)	-5.0
2021	107.0 (± 12.5)	107.0 (± 12.7)	0.0	271.0 (± 20.1)	270.0 (± 20.5)	-1.0
2022	116.0 (± 16.4)	116.0 (± 15.8)	0.0	270.0 (± 31.7)	259.0 (± 34.1)	-11.0
Average	115.5	115.8	0.3	270.3	265.5	-4.8

Table 4. Phenology metrics derived from TCNIRv for GF, 2019-2022. The gap is calculated as the metrics of NFS – SFS. Note that EOS at NFS is averagely 1.5 days later than that at SFS

GF (TCNIRv)	SOS (DOY)			EOS (DOY)		
	SFS	NFS	Gap	SFS	NFS	Gap
2019	117.0 (± 10.3)	118.0 (± 9.4)	+1.0	267.0 (± 19.2)	271.0 (± 19.7)	+4.0
2020	121.0 (± 9.9)	122.0 (± 14.5)	+1.0	266.0 (± 25.4)	268.0 (± 29.7)	+2.0
2021	106.0 (± 10.4)	107.0 (± 14.7)	+1.0	270.0 (± 16.9)	271.0 (± 22.6)	+1.0
2022	115.0 (± 11.7)	116.0 (± 21.2)	+1.0	264.0 (± 29.5)	263.0 (± 36.6)	-1.0
Average	114.8	115.8	+1.0	266.8	268.3	+1.5

Table 5. Phenology metrics derived from NIRv for ONP, 2019-2022. The gap is calculated as the metrics of NFS – SFS. Note that EOS at NFS is averagely 3.3 days earlier than that at SFS

ONP (NIRv)	SOS (DOY)			EOS (DOY)		
	SFS	NFS	Gap	SFS	NFS	Gap
2019	130.0 (± 10.7)	129.0 (± 7.9)	-1.0	271.0 (± 20.7)	265.0 (± 19.0)	-6.0
2020	141.0 (± 14.1)	139.0 (±11.6)	-2.0	244.0 (± 21.8)	245.0 (± 19.8)	+1.0
2021	123.0 (± 12.9)	123.0 (± 11.7)	0.0	270.0 (± 18.2)	267.0 (± 19.2)	-3.0
2022	134.0 (± 18.8)	133.0 (± 19.1)	-1.0	275.0 (± 20.8)	270.0 (± 20.8)	-5.0
Average	132.0	131.0	-1.0	265.0	261.8	-3.3

Table 6. Phenology metrics derived from TCNIRv for ONP, 2019-2022. The gap is calculated as the metrics of NFS – SFS. Note that EOS at NFS is averagely 2.8 days later than that at SFS

ONP (TCNIRv)	SOS (DOY)			EOS (DOY)		
	SFS	NFS	Gap	SFS	NFS	Gap
2019	129.0 (± 9.6)	129.0 (± 9.6)	0.0	266.0 (± 18.8)	268.0 (± 20.1)	+2.0
2020	140.0 (± 13.5)	139.0 (±14.4)	-1.0	243.0 (± 19.5)	249.0 (± 22.2)	+6.0
2021	123.0 (± 11.9)	123.0 (± 14.8)	0.0	267.0 (± 16.1)	269.0 (± 19.6)	+2.0
2022	133.0 (± 16.2)	134.0 (± 19.9)	+1.0	272.0 (± 19.4)	273.0 (± 21.0)	+1.0
Average	131.3	131.3	0.0	262.0	264.8	+2.8

IV. Discussion

In this study, we observed the differences in phenology metrics estimates using NIRv and TCNIRv. TCNIRv adopted a topographic correction conversion factor derived from the mathematical simplification of a canopy radiative transfer model, mitigating the effects of illumination conditions on NIRv. We observed that TCNIRv-derived EOS occurs earlier than NIRv-derived EOS, and the gap between them is larger in relatively rugged terrain (ONP) compared to relatively flat terrain (GF). These findings align with previous studies indicating that TCNIRv-derived EOS precedes NIRv-derived EOS (Chen *et al*., 2023b).

Then we compared the phenology metrics estimates, especially for EOS, with respect to slope orientation. Employing threshold methods for phenology metrics extraction, we considered uncertainties arising from arbitrary threshold settings by examining the distribution of phenology metrics derived from varying threshold, i.e. 15% to 50% with a 0.1% step. Then we examined exact DOY by setting threshold as 50%. While NIRv-derived EOS is significantly earlier at NFS compared to SFS (GF : DOY 270.3/265.5 for SFS/NFS; ONP : DOY 265/261.8 for SFS/NFS), TCNIRv-derived EOS at NFS is significantly delayed compared to SFS (GF : DOY 266.8/268.3 for SFS/NFS; ONP : DOY 262/264.8 for SFS/NFS). Additionally, we found that the gap (i.e., NFS-SFS) of TCNIRv-derived EOS between SFS and NFS (GF : +1.5 days; ONP : +2.8 days) is smaller than gap of NIRv-derived EOS between them (GF : -4.8 days; ONP : -3.3 days).

Our study has two main limitations. First, without data on other climate factor, we couldn't pinpoint the exact cause of these results in the study. Previous studies examined that plants at NFS have longer growing season length than that at SFS under specific condition, but these studies typically focus on semi-arid climates (Guerrero *et al*., 2016; Wang *et al*., 2023). Plant growth in semi-arid regions is dominantly affected by soil moisture, and soils at NFS are known to contain more moisture than soils at SFS due to sunlight exposure affecting soil moisture levels (Guerrero *et al*., 2016). However, to the best of our knowledge, such phenomena have not been studied in South Korea, and we were unable to obtain climate data segregated based on slope orientation for analysis of the relationship between climate and phenology metrics.

The other limitation of this research is the absence of data for validating results, such as gross primary production (GPP). While several LSP studies adopt GPP as an evaluation factor orientation (Caparros-Santiago *et al*., 2021), especially those derived from ground-level remote sensing products, our study sites were not equipped for these observations, making it challenging to obtain data considering slope orientation.

We suggest that future studies should aim to include validation data and analyze relationships with other climate factors. Also, to identify certain features of phenology estimation using TCNIRv with respect to topographic features, more samples with field observations are needed.

V. Conclusion

This is the first study to compare phenology metrics derived from TCNIRv between SFS and NFS. The implementation of topographic correction with TCNIRv revealed notable distinctions in the timing of EOS between NFS and SFS. Specifically, TCNIRv-derived EOS at NFS exhibited a significantly delay compared to SFS, while NIRv-derived EOS indicated an earlier occurrence at NFS. Additionally, the gap between SFS and NFS diminished after topographic correction. Our findings underscore the necessity of topographic correction in accurately estimating plant growth, particularly in diverse terrain conditions. This study paves the way for future investigations that integrate additional climate factors and employ a robust validation process, contributing to a comprehensive understanding of climate-carbon feedbacks in mountainous regions.

적 요

개엽기, 낙엽기 추정은 식물 생태 주기를 이해하는 데 매우 중요한 역할을 한다. 식물의 근적외선 반사 (NIRv)는 일차생산량(GPP)의 강력한 대리지표로 밝혀져 식물계절학 연구에 활발하게 가용되는 추세이다. 하지만 지형에 의한 반사도 왜곡 효과가 상쇄되지 않아 산악 지역의 지형 왜곡 효과에 민감하며 낙엽기를 추정하는 데 성능이 떨어진다. 지형 보정 NIRv (TCNIRv)는 지형 왜곡 효과와 관련된 한계점을 완화하기 위해 경로 길이 보정 방법을 사용한다. TCNIRv 는 낙엽기에 대해 NIRv 보다 더 정확한 값을 추정할 수 있다는 사실이 확인되었다. 지형 보정은 경사 및 사면 방향 같은 지형 속성과 연관성이 크기 때문에, 이번 연구에서는 광릉 수목원과 오대산 국립공원 같이 비교적 상이한 지형 특성을 가진 두 산악 지역을 대상으로 남사면과 북사면에서의 예측 결과를 비교하였다. 결과적으로, 두 연구지에서 TCNIRv 를 이용해 예측한 낙엽기는 북사면에서 남사면보다 지연되었고 (광릉 수목원: SFS/NFS - DOY 266.8/268.3; 오대산 국립공원: SFS/NFS - DOY 262/264.8), 이는 NIRv 의 결과와는 반대되는 예측 결과였다 (광릉 수목원: SFS/NFS - DOY 270.3/265.5; 오대산 국립공원: SFS/NFS - DOY 265/261.8). 또한 지형 보정 이후 남사면와 북사면 간의 낙엽기의 차이가 감소했다는 사실도 알 수 있었다 (광릉 수목원: SFS/NFS - DOY 270.3/265.5; 오대산 국립공원: SFS/NFS - DOY 265/261.8). 우리는 사면방향에 따라 식물 생장기를 예측했을 때, TCNIRv 를 이용한 낙엽기 추정에서 NIRv 를 이용해 예측한 결과와 차이점을 가진다고 결론 내렸다. 이로써 다양한 지형 조건에서 사면 별 식물 생장기를 추정하는 데 지형 보정이 필수적이라는 사실을 강조한다.

List of Abbreviations

LSP　　 : Land Surface Phenology
VI　　　 : Vegetation Index
NDVI　 : Normalized Difference Vegetation Index
NIR　　 : Near-Infrared Reflectance
NIRv　　: Near-Infrared Reflectance of Vegetation
TCNIRv : Topographically Corrected NIRv
GPP　　 : Gross Primary Production
SOS　　 : Start Of the Season
EOS　　 : End Of the Season
PLC　　 : Path Length Correction
SFS　　 : South Facing Slope
NFS　　 : North Facing Slope
DOY　　 : Day Of Year
(Internally introduced abbreviation within the paper below)
GF　　　: Gwangneung Forest
ONP　　 : Odaesan National Park

REFERENCES

Badgley, G., C. B. Field, and J. A. Berry, 2017: Canopy near-infrared reflectance and terrestrial photosynthesis. *Science Advances* **3**(3), e1602244. https://doi.org/doi:10.1126/sciadv.1602244

Baldocchi, D. D., Y. Ryu, B. Dechant, E. Eichelmann, K. Hemes, S. Ma, C. R. Sanchez, R. Shortt, D. Szutu, and A. Valach, 2020: Outgoing near-infrared radiation from vegetation scales with canopy photosynthesis across a spectrum of function, structure, physiological capacity, and weather. *Journal of Geophysical Research: Biogeosciences* **125**(7), e2019JG005534.

Caparros-Santiago, J. A., V. Rodriguez-Galiano, and J. Dash, 2021: Land surface phenology as indicator of global terrestrial ecosystem dynamics: A systematic review. *ISPRS Journal of Photogrammetry and Remote Sensing* **171**, 330-347. https://doi.org/10.1016/j.isprsjprs.2020.11.019

Chen, R., G. Yin, G. Liu, J. Li, and A. Verger, 2020: Evaluation and normalization of topographic effects on vegetation indices. *Remote Sensing* **12**(14), 2290. https://www.mdpi.com/2072-4292/12/14/2290

Chen, R., G. Yin, W. Zhao, B. Xu, Y. Zeng, G. Liu, and A. Verger, 2022: TCNIRv: Topographically corrected near-infrared reflectance of vegetation for

tracking gross primary production over mountainous areas. *IEEE Transactions on Geoscience and Remote Sensing* **60**, 1-10. https://doi.org/10.1109/TGRS.2022.3149655

Chen, R., G. Yin, W. Zhao, K. Yan, S. Wu, D. Hao, and G. Liu, 2023a: Topographic correction of optical remote sensing images in mountainous areas: A systematic review. *IEEE Geoscience and Remote Sensing Magazine,* 2-22. https://doi.org/10.1109/MGRS.2023.3311100

Chen, R., G. Yin, G. Liu, Y. Yang, C. Wang, Q. Xie, and A. Verger, 2023b: Correction of illumination effects on seasonal divergent NIRv photosynthetic phenology. *Agricultural and Forest Meteorology*, **339**, 109542. https://doi.org/10.1016/j.agrformet.2023.109542

Dash, J., and B. O. Ogutu, 2016: Recent advances in space-borne optical remote sensing systems for monitoring global terrestrial ecosystems. *Progress in Physical Geography* **40**(2), 322-351.

de Beurs, K. M., and G. M. Henebry, 2004: Land surface phenology, climatic variation, and institutional change: Analyzing agricultural land cover change in Kazakhstan. *Remote Sensing of Environment* **89**(4), 497-509. https://doi.org/10.1016/j.rse.2003.11.006

Florinsky, I., T. Skrypitsyna, and O. Luschikova, 2018: Comparative accuracy of the AW3D30 DSM, ASTER GDEM, and SRTM1 DEM: A case study on the Zaoksky testing ground, Central European Russia. *Remote Sensing Letters* **9**(7), 706-714.

Guerrero, F. J. D. T., A. Hinojosa-Corona, T. G. Kretzschmar, 2016: A comparative study of NDVI values between north- and south-facing slopes in a semiarid mountainous region. *IEEE Journal of Selected Topics in Applied Earth Observations and Remote Sensing* **9**(12), 5350-5356. https://doi.org/10.1109/JSTARS.2016.2618393

Horn, B. K., 1981: Hill shading and the reflectance map. *Proceedings of the IEEE* **69**(1), 14-47.

Huete, A., K. Didan, T. Miura, E. P. Rodriguez, X. Gao, and L. G. Ferreira, 2002: Overview of the radiometric and biophysical performance of the MODIS vegetation indices. *Remote Sensing of Environment* **83**(1-2), 195-213.

Karami, M., A. Westergaard-Nielsen, S. Normand, U. A. Treier, B. Elberling, and B. U. Hansen, 2018: A phenology-based approach to the classification of Arctic tundra ecosystems in Greenland. *ISPRS Journal of Photogrammetry and Remote Sensing*

146, 518-529.

Rodriguez-Galiano, V. F., J. Dash, and P. M. Atkinson, 2015: Characterising the land surface phenology of Europe using decadal MERIS data. *Remote Sensing* **7**(7), 9390-9409. https://www.mdpi.com/2072-4292/7/7/9390

Wang, H., D. Yakir, E. Rotenberg, 2023: Assessing the effectiveness of a central flux tower in representing the spatial variations in gross primary productivity in a semi-arid pine forest. *Agricultural and Forest Meteorology* **333**, 109415. https://doi.org/10.1016/j.agrformet.2023.109415

Wang, R., J. M. Chen, Z. Liu, Z., A. Arain, 2017: Evaluation of seasonal variations of remotely sensed leaf area index over five evergreen coniferous forests. *ISPRS Journal of Photogrammetry and Remote Sensing* **130**, 187-201. https://doi.org/10.1016/j.isprsjprs.2017.05.017

Wang, X., M. P. Dannenberg, D. Yan, M. O. Jones, J, S. Kimball, D. J. P. Moore, W. J. D. van Leeuwen, K. Didan, and W. K. Smith, 2020: Globally consistent patterns of asynchrony in vegetation phenology derived from optical, microwave, and fluorescence satellite data. *Journal of Geophysical Research: Biogeosciences* **125**(7), e2020JG005732. https://doi.org/10.1029/2020JG005732

Wang, X., J. Xiao, X. Li, G. Cheng, M. Ma, G. Zhu, M. Altaf Arain, T. Andrew Black, and R. S. Jassal, 2019: No trends in spring and autumn phenology during the global warming hiatus. *Nature Communications* **10**(1), 2389. https://doi.org/10.1038/s41467-019-10235-8

Wen, J., Q. Liu, Q. Liu, Q. Xiao, Q. and X. Li, 2009: Parametrized BRDF for atmospheric and topographic correction and albedo estimation in Jiangxi rugged terrain, China. *International Journal of Remote Sensing* **30**(11), 2875-2896. https://doi.org/10.1080/01431160802558618

White, M. A., P. E. Thornton, and S. W. Running, 1997: A continental phenology model for monitoring vegetation responses to interannual climatic variability. *Global Biogeochemical Cycles* **11**(2), 217-234. https://doi.org/10.1029/97GB00330

Yang, Y., R. Chen, G. Yin, C. Wang, G. Liu, A. Verger, A. Descals, I. Filella, and J. Peñuelas, 2022: Divergent performances of vegetation indices in extracting photosynthetic phenology for northern deciduous broadleaf forests. *IEEE Geoscience and Remote Sensing Letters* **19**, 1-5. https://doi.org/10.1109/LGRS.2022.3182405

Yang, Y., and F. Fan, 2023: Land surface phenology

and its response to climate change in the Guangdong-Hong Kong-Macao Greater Bay Area during 2001−2020. *Ecological Indicators* **154**, 110728. https://doi.org/10.1016/j.ecolind.2023.110728

Yin, G., A. Li, S. Wu, W. Fan, Y. Zeng, K. Yan, B., Xu, J. Li, and Q. Liu, 2018: PLC: A simple and semi-physical topographic correction method for vegetation canopies based on path length correction. *Remote Sensing of Environment* **215**, 184-198. https://doi.org/10.1016/j.rse.2018.06.009

Yin, G., A. Verger, I. Filella, A. Descals, and J. Peñuelas, 2020a: Divergent estimates of forest photosynthetic phenology using structural and physiological vegetation indices. *Geophysical Research Letters* **47**(18), e2020GL089167.

Yin, G., L. Ma, W. Zhao, Y. Zeng, B. Xu, and S. Wu, 2020b: Topographic correction for Landsat 8 OLI vegetation reflectances through path length correction: A comparison between explicit and implicit methods. *IEEE Transactions on Geoscience and Remote Sensing* **58**(12), 8477-8489. https://doi.org/10.1109/TGRS.2020.2987985

Zeng, L., B. D. Wardlow, D. Xiang, S. Hu, and D. Li, 2020: A review of vegetation phenological metrics extraction using time-series, multispectral satellite data. *Remote Sensing of Environment* **237**, 111511. https://doi.org/10.1016/j.rse.2019.111511

Zhang, Y., R. Commane, S. Zhou, A. P. Williams, and P. Gentine, 2020: Light limitation regulates the response of autumn terrestrial carbon uptake to warming. *Nature Climate Change* **10**(8), 739-743. https://doi.org/10.1038/s41558-020-0806-0